Published in final edited form as:
Nat Med. 2013 November ; 19(11): 1518–1523. doi:10.1038/nm.3328.

Coordinate activation of Shh and PI3K signaling in PTEN-deficient glioblastoma: new therapeutic opportunities

Mariella Gruber-Filbin[1,2,3], **Sukriti K. Dabral**[1,2], **Maria F. Pazyra-Murphy**[1,2], **Shakti Ramkissoon**[4,5], **Andrew L. Kung**[1,6], **Ekaterina Pak**[1,2], **Jarom Chung**[1,2], **Matthew A. Theisen**[4], **Yanping Sun**[6], **Yoko Franchetti**[7], **Yu Sun**[1,2], **David S. Shulman**[1], **Navid Redjal**[8], **Barbara Tabak**[4], **Rameen Beroukhim**[4], **Qi Wang**[1], **Jean Zhao**[1], **Marion Dorsch**[9], **Silvia Buonamici**[10], **Keith L. Ligon**[4,5], **Joseph F. Kelleher**[10], and **Rosalind A. Segal**[1,2]

[1]Depts of Cancer Biology and Pediatric Oncology, Dana-Farber Cancer Institute and Children's Hospital Boston, Harvard Medical School, Boston, MA 02115, USA

[2]Dept of Neurobiology, Harvard Medical School, Boston, MA 02115, USA

[3]Dept of Pediatrics and Adolescent Medicine, Medical University of Vienna, Vienna, Austria

[4]Dept of Medical Oncology, Center for Molecular Oncologic Pathology, Dana-Farber Cancer Institute, Boston, MA 02215, USA

[5]Depts of Pathology, Children's Hospital Boston and Brigham and Women's Hospital, Harvard Medical School, Boston, MA 02115, USA

[6]Lurie Family Imaging Center, Dana-Farber Cancer Institute, Boston, MA 02115, USA

[7]Dept of Biostatistics and Computational Biology, Dana-Farber Cancer Institute and Harvard School of Public Health, Boston, MA 02115, USA

[8]Dept of Neurological Surgery, Massachusetts General Hospital, Harvard Medical School, Boston, MA 02114, USA

[9]Sanofi-Aventis, Cambridge, MA 02139, USA

[10]Novartis Institutes for Biomedical Research, Cambridge, MA 02139, USA

Abstract

In glioblastoma, PI3kinase (PI3K) signaling is frequently activated by loss of the tumor suppressor PTEN[1]. However, it is not known whether inhibiting PI3K represents a selective and effective approach for treatment. Here we interrogate large databases and find that Shh signaling is activated in PTEN-deficient glioblastoma. We demonstrate that Shh and PI3K pathways synergize to promote tumor growth and viability in human PTEN-deficient glioblastomas. A combination of PI3K and Shh signaling inhibitors not only suppresses activation of both pathways, but also abrogates S6kinase signaling. Accordingly, simultaneously targeting both pathways results in mitotic catastrophe and tumor apoptosis, and dramatically reduces growth of PTEN-deficient glioblastomas *in vitro* and *in vivo*. The drugs tested here appear safe in humans; therefore this combination may provide new targeted treatment for glioblastoma.

Contact: Correspondence and requests for materials should be addressed to rosalind_segal@dfci.harvard.edu.

Author contributions

Manuscript written by MGO, SKD, EP, RAS with input from all authors. MGO, SKD, EP, JC, MFP-M, YS executed *in vitro* studies and analyzed *in vitro* and *in vivo* studies. ALK, YS, YF, JFK, SB and MD performed *in vivo* studies. MAT, KLL, SR generated GBM lines, analyzed tumor pathology. DSS, NR initiated these studies. BT, RB analyzed databases. JZ, QW provided shPTEN.

Microarray data in Supplementary Figure 4 deposited in NCBI's Gene Expression Omnibus; accessible through GEO Series accession number GSE49416 (http://www.ncbi.nlm.nih.gov/geo/query/acc.cgi?acc=GSE49416).

Glioblastoma multiforme (GBM) is the most common malignant primary brain tumor. Currently average time from diagnosis to death is 15–18 months[2], therefore new approaches are needed[3]. 36% of GBMs harbor loss or inactivation of Phosphatase and tensin homolog (PTEN)[1], a lipid phosphatase that is a key negative regulator of PI3K signaling. However, it is unclear whether tumors deficient for PTEN are susceptible to PI3K inhibitors[4,5].

Here we describe a therapeutic approach that targets PTEN-deficient GBMs. In two large data sets, *pten* mRNA expression varies more than ten-fold among GBMs[6]. We divided a dataset of 100 GBMs[6], and the TCGA dataset of over 400 GBMs[7] into those that express low levels of *pten* versus all other tumors (Supplementary Fig. 1a). In both datasets, GBMs with decreased *pten* exhibit increased Shh pathway activation, assessed by expression of *gli1* and *gli2*, which encode transcription factors critical for Shh signaling (Fig. 1a, Supplementary Fig. 1b). Moreover, *pten* expression negatively correlates with combined mRNA expression of *gli1* and *gli2* across each dataset (Spearman Correlation coefficient −0.23, p = 0.02 and −0.23226, $p = 2x10^{-6}$ respectively). Further analysis of TCGA data demonstrates that *gli2* expression is higher in tumors with *pten* copy loss (Fig. 1b, Supplementary Fig. 1c), and, as expected, *pten* expression correlates with *pten* copy number. These data indicate that PTEN-deficient GBMs exhibit activation of Shh signaling, in addition to the known activation of PI3K cascades.

We tested the effects of selective PI3K and Shh inhibitors on neurosphere cultures from a human PTEN-deficient GBM (hBT70), and a PTEN-expressing GBM (hBT75)[8] (Fig. 1d). Neurosphere cultures recapitulate critical features of primary tumors, including somatic mutations, antigenic properties, tumor initiation and angiogenic activity[9]. Treatment with PI3K inhibitor NVP-BKM120[4] at 100 nM (IC50 52–99, 166, 116 nM for p110α, β, γ)[5] did not alter cell viability of PTEN-deficient or PTEN-expressing neurospheres (Fig. 1d). No effect on viability was seen when we treated with NVP-LDE225, an inhibitor of Smoothened (Smo) which prevents Shh signaling[10]. In contrast, in PTEN-deficient GBM neurosphere cultures only, a significant reduction in viability was seen with combination of BKM120 and LDE225 at multiple doses of inhibitors; responses to PI3K inhibitors alone were observed at high doses (Fig. 1d,e, Supplementary Fig. 1d). Using varying doses of several inhibitors targeting PI3K and Shh pathways[11], we consistently observed a synergistic decrease in cell viability with combination therapy (Fig. 1e, Supplementary Fig. 1e,f). This effect was only seen with continuous treatment (Supplementary Fig. 1g). Thus simultaneous inhibition of PI3K and Shh pathways reduces viability of human PTEN-deficient GBMs, as demonstrated using several distinct targeted drugs.

We analyzed responses to combination therapy in monolayer cultures of hBT70 and two additional PTEN-deficient tumors (hBT112, hBT145) (Fig 1c)[12]. Combination therapy led to efficacious and synergistic reduction in viability in all PTEN-deficient tumors tested (Fig. 1f) (two-way ANOVA factorial interaction, $F = 10.27$, $DFn = 1$, $DFd = 8$, $p = 0.0125$), but did not alter growth in PTEN-expressing GBMs (Fig. 1c, g). As human GBMs vary in several additional characteristics (Supplementary Fig. 1h) we asked whether PTEN expression is a critical determinant of response. Two different shRNAs against *pten* introduced in two distinct PTEN-expressing human GBMs decreased PTEN levels by 50–70% (Fig. 1h). Acute reduction of PTEN increases *gli1* and *gli2* expression (Fig. 1i), while acute overexpression of PTEN decreases these Shh pathway components (Supplementary Fig. 1i). Notably, when PTEN expression is stably reduced in two distinct GBM tumors, combination therapy with BKM120 and LDE225 decreases viability of previously resistant cells (Fig. 1j). Thus PTEN expression is not merely correlative for response, but has a causative role as well.

Based on these promising results we analyzed PTEN-deficient tumors *in vivo*, using an orthotopic xenograft model[13]. We intracranially,injected $1x10^6$ human GBM cells (hBT112) expressing luciferase and followed tumor size with bioluminescence[13]. We initiated treatment only after tumors showed exponential growth. Mice treated with vehicle or LDE225 exhibited rapid increases in bioluminescence (Fig. 2a). BKM120 treatment initially slowed tumor growth, however this effect was transient. In striking contrast, mice treated with combination therapy showed stable bioluminescence throughout the experiment, indicating dramatically reduced tumor growth ($p = 0.026$, compared to vehicle) (Fig. 2a). Similar results were seen in a second tumor tested *in vivo* (hBT145) (Fig. 2b). Moreover, while both BKM120 and combination therapy treated groups show improved survival compared to vehicle and LDE225 treated groups (Fig. 2c), tumor burden in animals that survived to late time points is reduced in mice treated with combination therapy (Fig. 2d).

Consistent with bioluminescence studies, MRIs and histological examination show that combination therapy diminished tumor size (Fig. 2e,f) and decreased dissemination of tumor cells (Fig. 2f) as assessed by staining for human NuMA (nuclear mitotic apparatus protein).

To examine the cellular basis for synergistic effects of combination treatment, we labeled glioblastoma cells with DiI (1,1′-dioctadecyl-3,3,3′,3′-tetramethylindocarbocyanine perchlorate), and imaged individual cells over time (Fig. 3a). Combination therapy decreases proliferation and increases cell death (Fig. 3b). Accordingly, combination therapy increases apoptosis both *in vitro*, demonstrated by activated caspase-3 (Fig. 3c,d, Supplementary Fig. 2a) and *in vivo*, demonstrated by TUNEL stain of GBM xenografts (Fig. 3e,f). Combination therapy also affects tumor cell morphology: *In vitro*, combination therapy reduces cell size (Supplementary Fig. 2b) and results in abnormal mitotic spindles, in which chromosomes distributed in a rosette-like pattern surround centrally located centrosomes (Fig. 3g,h). *In vivo*, combination therapy-treated GBM cells appeared smaller in size, with frequent pyknotic nuclei and aberrant mitotic figures (Fig. 3i, Supplementary Fig. 2c). Mitotic abnormalities might engender mitotic catastrophe[14], thereby contributing to diminished tumor growth. Indeed, in combination therapy, many dividing cells produce two daughters that rapidly die (Supplementary Fig. 2d). Thus, combination treatment causes mitotic abnormalities and apoptosis *in vitro* and *in vivo*.

Combination therapy clearly achieves targeted responses: BKM120, alone or combined with LDE225, decreases phosphorylation of Akt, the kinase activated by PIP3 phospholipids[15] (Fig. 4a, Supplementary Fig. 3a). Consistent with data that *gli* levels are high in *pten*–deficient GBMs, *gli1* mRNA is readily detected in hBT112 cells, and LDE225 decreases expression of *gli1 and ptc1* (Fig. 4b). This effect of LDE225 is potentiated when combined with BKM120 (Fig. 4c, Supplementary Fig. 3b).

An inhibitor of the PI3K–regulated mTOR complex (NVP-RAD001)[16] significantly reduced tumor cell viability when combined with LDE225 (Fig. 4d), indicating that the pathways intersect further downstream. Inhibition of S6kinase (S6K), which is regulated by mTOR, could explain decreased cell size observed with combination therapy[15, 17]. In cultured GBM cells, both BKM120 and LDE225 alone reduce pS6K and pS6, and these effects are potentiated in combination therapy (Fig. 4e, Supplementary Fig. 3c). Similarly, *in vivo* both LDE225 and combination treatment reduced pS6 (Fig. 4f,g). Stimulation of GBM cells with SAG, a Smoothened agonist[18], causes dose-dependent increases in pS6, implicating the Shh pathway in S6K activation (Fig. 4h). Furthermore, a small molecule inhibitor of S6K (PF 4708671)[19] leads to dose-dependent decreases in pS6 and tumor cell viability (Fig. 4i, Supplementary Fig. 3d), suggesting that S6K represents a critical interaction node for combination therapy. Combination therapy also synergistically decreases cyclinD1, which is regulated by PI3K, Shh and S6K pathways[20,21](Supplementary Fig. 3e. Thus, while

BKM120 and LDE225 each successfully attack appropriate targets in PTEN-deficient GBM cells, both PI3K- and Shh signaling must be targeted to maximally diminish S6K activity and repress tumor growth.

To identify additional consequences of combination therapy on a genome-wide scale, we performed Affymetrix microarrays with two different PTEN-deficient GBMs treated with single drugs or combination therapy. Genes significantly affected by combination therapy in hBT70 and/or hBT112 (Supplementary Fig. 3f, Supplementary Table 1, include several genes implicated in GBM prognosis, or identified as targets of Shh, PI3K or S6 pathways [22–24](Figure 4j).

The studies presented here indicate that Shh signaling and PI3K cascades are both activated in PTEN-deficient GBMs, and therapies that target only PI3K have limited efficacy in these tumors[25]. Instead, a combination of PI3K and Shh signaling inhibitors successfully targets both pathways and achieves a synergistic effect on S6K signaling. Combination therapy causes apoptosis as well as mitotic catastrophe, and dramatically reduces tumor growth *in vitro* and *in vivo*.

Activation of Shh signaling has previously been reported in GBMs[26,27]. Here we find that expression of gli transcription factors correlates with both *pten* mRNA levels and *pten* copy number in large GBM databases. Our data indicate a causal connection between PTEN and Shh signaling and identify S6K signaling as a critical node of interaction[28–31] (Figure 4j). In the absence of PTEN, decreased degradation of PIP3 lipids results in activation of Akt, mTOR and S6K; S6K activity in turn enhances *gli*-dependent transcription[17,32–34] Stimulation of the Shh receptor, Smo, further enhances S6K signaling. Accordingly PTEN-deficiency increases PI3K, Shh and S6K signaling, and so a combination of PI3K and Shh inhibitors results in apoptotic death of PTEN-deficient hGBM cells.

Previous studies suggest that high doses with inhibitors of either the Shh or PI3K pathway reduce GBM neurosphere growth and/or colony formation [4,35–38] Here we show efficacy using doses of the PI3K inhibitor, BKM120 and the Shh pathway inhibitor, LDE225 achievable *in vivo* through oral administration. These drugs cross the blood-brain-barrier, have acceptable toxicity profiles and have now entered clinical trials [5,39,40]. Our results indicate the need to monitor PTEN status and pS6K activation in clinical studies and highlight the importance of testing these agents as combination therapy for glioblastoma[39,40].

Methods

Genomic Analysis

GEO database was used to examine *pten*, *gli1* and *gli2* in 100 high grade gliomas (H. Phillips, GEO Data Set GDS1815)[6]. Mean robust Z-score of *gli1* or *gli2* was determined for the set of tumors with lower *pten* expression (20–40% of tumors), and for the rest of the tumors with higher *pten* expression. Student's t-test was used to determine whether differences in *gli1* or *gli2* between these groups was significant. Data in Supplementary Fig 1a use a cut off of 22% (Supplementary Figure 1b); this difference was also significant ($p < 0.05$) for *gli1* and *gli2* using a cutoff at 34 or 39%. Similar analysis was carried out for TCGA data (LBL) in Figure 1a. *pten* copy number from TCGA[7], was categorized as copy loss (log2 ratio less than −0.3) or copy neutral. The −0.3 threshold represents a minimum in copy number distribution (Supplementary Figure 1b).

GBMs

All human subjects work was reviewed by the Institutional Review Board Committees of the Brigham and Women's Hospital and Dana-Farber Cancer Institute for appropriate use, that informed consent was obtained from all subjects when required, and appropriate waiver of consent requirements was obtained for minimal risk studies.

Animal studies

All experimental procedures were done in accordance with the National Institutes of Health guidelines and were approved by the Dana-Farber Cancer Institutional Animal Care and Use Committee.

GBMs in vitro

Human GBM tumor initiating cell lines (hBT112, hBT145, hBT188, hBT239) were derived from BWH patients according to IRB approved protocols. hBT70 and hBT75 lines are from C. David James[8] (UCSF). Cells from glioblastoma biopsies were implanted into nu/nu mice. Dissected xenografts were processed as described[8]. For adherent conditions, cells were cultured as described[12]. All cultures were grown in NS-A stem cell media (Stem Cell Technologies) with EGF (20 ng ml^{-1}), bFGF (20 ng ml^{-1}), 0.2% Heparin (1 μl ml^{-1}). Viability was determined by Trypan Blue exclusion or by CellTiter-Glo Luminescent Cell Viability Assay (Promega) at the end of treatment (day 7 for monolayer, day 14 for neurosphere assays). PTEN knock-down was achieved in hBT188 and hBT239 cultures after 48h infection with lentivirus expressing one of two distinct shRNAs to pten. Cells were used after 7 d Puromycin selection (1 μg ml^{-1}) in assays of viability, immunoblotting and real time RT-PCR. PTEN overexpression was achieved in hBT112 cultures after 48h infection with a retrovirus expressing full length pten. Cells were used after 1 d Puromycin selection (1 μg ml^{-1}) in assays of real time RT-PCR.

Live imaging

Human GBM tumor initiating cells (hBT70) were stained with DiI (Vybrant Multicolor Cell-labelling Kit, Invitrogen) for 20 min at 37 °C, then mixed with unlabeled hBT70 cells, and plated on laminin-coated (10 μg ml^{-1}, Invitrogen) 12-well plates. 24 h after plating, drugs or vehicle was added as indicated. Dishes were placed within an incubation chamber fitted around the stage of an inverted microscope (Nikon Eclipse Ti). For nine fields per well, images for phase-contrast and fluorescent signal were captured with an XYZ stage-control system every 15 min over 120 h. Time-lapse images were analyzed with NIS Elements AR 3.10 software.

In vivo experiments

For orthotopic transplants, hBT112 or hBT145 neurospheres expressing luciferase[13] were dissociated and resuspended in HBSS at 1x10^6 cells/μl. One μl was injected stereotactically (coordinates: x = −2, y = 0,z = −2) into nu/nu mouse brains. After 6 weeks, animals were imaged weekly. Animals with increasing BLI were randomly assigned to four groups. Drugs were administered by oral gavage once daily; ten mice received vehicle control, ten mice LDE225 at 60 mg kg^{-1}, ten mice BKM120 at 30 mg kg^{-1} and ten mice the combination of LDE225 and BKM120, with 30 min between dosing of the two drugs. MRIs were performed on two animals per group at the end of treatment on day 65 (vehicle and LDE225) and day 77 (BKM120 and combo). T2 weighted images were acquired, 3D-rendered models were generated and tumor volume was measured using 3D Slicer with a thresholding method[13]. Animals were euthanized when ill.

Inhibitors

NVP-LDE225, NVP-BKM120, NVP-LEQ506 and NVP-RAD001 were from Novartis. NVP-LDE225, NVP-BKM120 were formulated as diphosphate salt in 0.5% methylcellulose and 0.5% Tween 80 (Fisher) for *in vivo* studies. For *in vitro* studies NVP-LDE225, NVP-BKM120, NVP-LEQ506 and NVP-RAD001 were suspended in DMSO and used at the concentrations indicated. GDC-0941 was from Sai Advantium Pharma and ShangHai Biochempartner. PF-4708671 was a generous gift from Nathanael Gray. Cyclopamine was from LC laboratories.

ShRNA for pten

hBT188 and hBT239 neurospheres were cultured as monolayer on laminin[12]. Lentivirus (Sh-Control) targets Luciferase. Targeting Sequence for sh-PTEN1 is CCACAGCTAGAACTTATCAAA, for sh-PTEN2 is AGCCGCTATGTGTATTATTAT. Protamine was included during lentiviral infection; following infection cells were selected in puromycin 1 μg ml^{-1} for 1 week.

Immunoblots

GBM tumor initiating cells were lysed in modified RIPA buffer (50 mM NaTris ph 7.4, 150 mM NaCl, 1% v/v NP-40, 0.25% Na-Deoxycholate, 1 mM DTT, 10 mM NaF, 1 mM active Na-Vanadate, 1 mM PMSF, 1x Proteinase Inhibitor). Lysates were separated by 4–12% SDS-PAGE. Antibodies used: rabbit anti-PTEN (1:1000) rabbit anti-Akt (1:1000), rabbit anti-phospho Akt (Ser473) (1:2000), rabbit anti-phospho Akt (Thr308) (1:1000), rabbit anti-cyclin D1 (1:5000), rabbit anti-p70 S6 kinase (1:1000), rabbit anti-phospho p70 S6 kinase (1:1000), mouse anti-S6 ribosomal protein (1:1000), rabbit anti-phospho S6 ribosomal protein (1:1000), and rabbit anti-actin (1:1000). Anti-cyclinD1 ab was from Millipore; all other antibodies were from Cell Signaling Technologies. Bands were visualized with secondary antibodies conjugated to HRP (1:10,000; Bio-Rad) and ECL Western Blotting Detection Reagents (Amersham); band intensity was quantified with ImageJ 1.42q and normalized to actin.

Immunocytochemistry

hBT70 cells were plated on laminin-coated cover slips and treated as indicated for 7 d. Cells were fixed for 15 min in 4% PFA, blocked in 10% normal goat serum, 1% bovine serum albumin, and 0.1% TritonX-100 in PBS for 30 min at room temperature before staining for activated caspase-3, or fixed at −20C for 10 min in pre-cooled 100% methanol, permeabilized at RT for 5 min in 0.2% Triton X-100 and blocked at RT for 30 min in 5% bovine serum albumin and 0.1% Triton X-100 for spindle staining. Samples were incubated with primary antibodies for 2 h at room temperature, then with anti-rabbit Alexa Fluor 488 (Invitrogen, 1:800) or anti-mouse AlexaFluor 546 (Invitrogen, 1:800) and DAPI for 1.5 h at room temperature. All cover slips were mounted using ProLong Gold Antifade Reagent (Invitrogen). Primary antibodies used were: rabbit anti-activated caspase-3 (Abcam ab83847, 1:1000), rabbit anti-γ-tubulin (Sigma Aldrich #T5192, 1:400) and mouse anti-acetylated tubulin (Sigma Aldrich #6793, 1:800).

Images were obtained with a Nikon E800 microscope, CoolSnap EZ camera and NIS Imaging software using a 40x oil objective for γ-tubulin and acetylated tubulin and a 20x objective for activated caspase-3. Images of spindles were acquired using a 100x objective, Yokogawa Spinning Disk Confocal microscope, Orca ER camera and Andor iQ 2.3 software.

Immunohistochemistry of in vivo tumors

Specimens were fixed in 10% buffered-formalin, and embedded in paraffin. Five-micron sections were stained with hematoxylin and eosin (H&E) or used for immunohistochemical studies. After antigen retrieval (citrate, high temperature) NuMA antibody was used (Epitomics, S2825, 1:200), Phospho S6 (Cell Signaling #2211S, 1:200) and visualized using the Envision Plus Detection System (Dako, Carpinteria, CA). Neuropathologists performed all evaluation and interpretation of brain sections (KL, SR). TUNEL staining was performed using the DeadEnd Fluorometric TUNEL System (Promega).

Real Time RT-PCR

GBM tumor initiating cells were collected and lysed in either RNAlater (Life Technologies) or Buffer RLT (Qiagen) and RNA was isolated with RNeasy Plus Mini kit (Qiagen). Reverse Transcription was performed with a High Capacity cDNA Reverse Transcription Kit (Applied Biosystems). Quantitative real-time RT-PCR was performed using Taqman Gene expression assays for *human pten* (Hs_02621230_s1), *human gli1* (Hs00171790_m1), *human gli2* (Hs_002579771_m1), *human ptch1* (Hs00181117_m1), and *human gapdh* (TaqMan Pre-developed Assay reagents). Each analysis was performed in triplicate, was normalized to *gapdh* levels for each samples.

Microarray analysis

RNA was isolated as described from hBT112 and hBT70 cells after 5 d of treatment, then applied to Affymetrix Human Genome U133A 2.0 Arrays by the DFCI microarray facility http://chip.dfci.harvard.edu. Biological duplicate samples were tested; arrays were visualized and analyzed using dChip software (http://www.biostat.harvard.edu/complab/dchip).

Statistical Analysis

All analysis was done using Microsoft Excel or Prism GraphPad 5.00 for Mac OS (San Diego California, www.graphpad.com), except for analysis of tumor growth in vivo, which was done using SAS 9.2 (SAS Institute Inc., Cary, NC). Synergistic effects of protein, mRNA or viability were analyzed by two-way ANOVA factorial design with Bonferroni post-test. Tests of efficacy were done using one-way ANOVA with Bonferroni post-test, student's two-tailed, type2 t-test, or z-test as indicated.

To combine multiple experiments, in each experiment results were normalized to the associated vehicle control before calculating mean and SEM.

For hBT112 *in vivo* experiments, normality was checked for all measurements using the Kolmogorov-Smirnov test, analysis of covariance and analysis of covariance tests were performed to explore treatment group effect as well as essential covariates among baseline weight, baseline log bioluminescence, and relative percent change of weight. In longitudinal modeling, five forms of linear mixed models were considered: 1) linear mixed model with random intercept, 2) individual linear mixed model with random intercept, 3) random regression model, 4) random regression model where random slope and intercept are assumed to be independent, and 5) linear mixed model where a within-subject covariance-variance structure is specified. Under respective models, group effect (categorized as vehicle-treated control, BKM120, LDE225, and combination of BKM120 and LDE225) was introduced as an independent variable, and we examined different combinations of the covariates and variance-covariance specifications (unstructured, 1-autoregressive, and compound symmetry). Among all the fit models, the best model was selected based on

Akaike information criterion (AIC) and significance of covariates. In order to make an inference on group effect, contrast tests were performed using the selected best model.

Supplementary Material

Refer to Web version on PubMed Central for supplementary material.

Acknowledgments

We thank V. Monrose, K. Jones for technical assistance and C. Stiles for helpful discussions. This work supported by an APART-fellowship of the Austrian Academy of Sciences (MGO), grants from NIH (RAS) and Novartis Pharmaceuticals.

This work supported in part by grants from Novartis Institute of BioMedical Research. JK is employee of, and RAS had consulting agreement with, Novartis Institute of Biomedical Research.

References

1. Cerami E, Demir E, Schultz N, Taylor BS, Sander C. Automated network analysis identifies core pathways in glioblastoma. PLoS One. 2010; 5:e8918. [PubMed: 20169195]
2. Stupp R, et al. Radiotherapy plus concomitant and adjuvant temozolomide for glioblastoma. N Engl J Med. 2005; 352:987–996. [PubMed: 15758009]
3. Quant EC, Wen PY. Novel medical therapeutics in glioblastomas, including targeted molecular therapies, current and future clinical trials. Neuroimaging Clin N Am. 2010; 20:425–448. [PubMed: 20708556]
4. Koul D, et al. Antitumor activity of NVP-BKM120--a selective pan class I PI3 kinase inhibitor showed differential forms of cell death based on p53 status of glioma cells. Clin Cancer Res. 2012; 18:184–195. [PubMed: 22065080]
5. Maira SM, et al. Identification and characterization of NVP-BKM120, an orally available pan-class I PI3-kinase inhibitor. Mol Cancer Ther. 2012; 11:317–328. [PubMed: 22188813]
6. Phillips HS, et al. Molecular subclasses of high-grade glioma predict prognosis, delineate a pattern of disease progression, and resemble stages in neurogenesis. Cancer Cell. 2006; 9:157–173. [PubMed: 16530701]
7. Comprehensive genomic characterization defines human glioblastoma genes and core pathways. Nature. 2008; 455:1061–1068. [PubMed: 18772890]
8. Pandita A, Aldape KD, Zadeh G, Guha A, James CD. Contrasting in vivo and in vitro fates of glioblastoma cell subpopulations with amplified EGFR. Genes Chromosomes Cancer. 2004; 39:29–36. [PubMed: 14603439]
9. Venere M, Fine HA, Dirks PB, Rich JN. Cancer stem cells in gliomas: identifying and understanding the apex cell in cancer's hierarchy. Glia. 2011; 59:1148–1154. [PubMed: 21547954]
10. Pan S, et al. Discovery of NVP-LDE225, a Potent and Selective Smoothened Antagonist. ACS Medicinal Chemistry Letters. 2010; 1:130–134.
11. Folkes AJ, et al. The identification of 2-(1H-indazol-4-yl)-6-(4-methanesulfonyl-piperazin-1-ylmethyl)-4-morpholin-4-yl-t hieno[3,2-d]pyrimidine (GDC-0941) as a potent, selective, orally bioavailable inhibitor of class I PI3 kinase for the treatment of cancer. J Med Chem. 2008; 51:5522–5532. [PubMed: 18754654]
12. Pollard SM, et al. Glioma stem cell lines expanded in adherent culture have tumor-specific phenotypes and are suitable for chemical and genetic screens. Cell Stem Cell. 2009; 4:568–580. [PubMed: 19497285]
13. Rubin JB, et al. A small-molecule antagonist of CXCR4 inhibits intracranial growth of primary brain tumors. Proc Natl Acad Sci U S A. 2003; 100:13513–13518. [PubMed: 14595012]
14. Vakifahmetoglu H, Olsson M, Zhivotovsky B. Death through a tragedy: mitotic catastrophe. Cell Death Differ. 2008; 15:1153–1162. [PubMed: 18404154]
15. Manning BD. Balancing Akt with S6K: implications for both metabolic diseases and tumorigenesis. J Cell Biol. 2004; 167:399–403. [PubMed: 15533996]

16. Dancey JE. Inhibitors of the mammalian target of rapamycin. Expert Opin Investig Drugs. 2005; 14:313–328.
17. Tandon P, et al. Requirement for ribosomal protein S6 kinase 1 to mediate glycolysis and apoptosis resistance induced by Pten deficiency. Proc Natl Acad Sci U S A. 2011; 108:2361–2365. [PubMed: 21262837]
18. Chen JK, Taipale J, Young KE, Maiti T, Beachy PA. Small molecule modulation of Smoothened activity. Proc Natl Acad Sci U S A. 2002; 99:14071–14076. [PubMed: 12391318]
19. Choi HN, et al. Inhibition of S6K1 enhances glucose deprivation-induced cell death via downregulation of anti-apoptotic proteins in MCF-7 breast cancer cells. Biochem Biophys Res Commun. 2013; 432:123–128. [PubMed: 23376066]
20. Kenney AM, Rowitch DH. Sonic hedgehog promotes G(1) cyclin expression and sustained cell cycle progression in mammalian neuronal precursors. Mol Cell Biol. 2000; 20:9055–9067. [PubMed: 11074003]
21. Liang J, Slingerland JM. Multiple roles of the PI3K/PKB (Akt) pathway in cell cycle progression. Cell Cycle. 2003; 2:339–345. [PubMed: 12851486]
22. Barbus S, et al. Differential retinoic acid signaling in tumors of long- and short-term glioblastoma survivors. J Natl Cancer Inst. 2011; 103:598–606. [PubMed: 21346226]
23. Lee EY, et al. Hedgehog pathway-regulated gene networks in cerebellum development and tumorigenesis. Proc Natl Acad Sci U S A. 2010; 107:9736–9741. [PubMed: 20460306]
24. Masi A, et al. hERG1 channels are overexpressed in glioblastoma multiforme and modulate VEGF secretion in glioblastoma cell lines. Br J Cancer. 2005; 93:781–792. [PubMed: 16175187]
25. Workman P, Clarke PA, Raynaud FI, van Montfort RL. Drugging the PI3 kinome: from chemical tools to drugs in the clinic. Cancer Res. 2010; 70:2146–2157. [PubMed: 20179189]
26. Xu Q, Yuan X, Liu G, Black KL, Yu JS. Hedgehog signaling regulates brain tumor-initiating cell proliferation and portends shorter survival for patients with PTEN-coexpressing glioblastomas. Stem Cells. 2008; 26:3018–3026. [PubMed: 18787206]
27. Becher OJ, et al. Gli activity correlates with tumor grade in platelet-derived growth factor-induced gliomas. Cancer Res. 2008; 68:2241–2249. [PubMed: 18381430]
28. Castellino RC, et al. Heterozygosity for Pten promotes tumorigenesis in a mouse model of medulloblastoma. PLoS One. 2010; 5:e10849. [PubMed: 20520772]
29. Buonamici S, et al. Interfering with resistance to smoothened antagonists by inhibition of the PI3K pathway in medulloblastoma. Sci Transl Med. 2010; 2:51ra70.
30. Riobo NA, Lu K, Ai X, Haines GM, Emerson CP Jr. Phosphoinositide 3-kinase and Akt are essential for Sonic Hedgehog signaling. Proc Natl Acad Sci U S A. 2006; 103:4505–4510. [PubMed: 16537363]
31. Kenney AM, Widlund HR, Rowitch DH. Hedgehog and PI-3 kinase signaling converge on Nmyc1 to promote cell cycle progression in cerebellar neuronal precursors. Development. 2004; 131:217–228. [PubMed: 14660435]
32. Mizuarai S, Kawagishi A, Kotani H. Inhibition of p70S6K2 down-regulates Hedgehog/GLI pathway in non-small cell lung cancer cell lines. Mol Cancer. 2009; 8:44. [PubMed: 19575820]
33. Evangelista M, et al. Kinome siRNA screen identifies regulators of ciliogenesis and hedgehog signal transduction. Sci Signal. 2008; 1:ra7. [PubMed: 18827223]
34. Wang Y, et al. The crosstalk of mTOR/S6K1 and Hedgehog pathways. Cancer Cell. 2012; 21:374–387. [PubMed: 22439934]
35. Eimer S, et al. Cyclopamine cooperates with EGFR inhibition to deplete stem-like cancer cells in glioblastoma-derived spheroid cultures. Neuro Oncol. 2012; 14:1441–1451. [PubMed: 23104476]
36. Ferruzzi P, et al. In vitro and in vivo characterization of a novel Hedgehog signaling antagonist in human glioblastoma cell lines. Int J Cancer. 2012; 131:E33–44. [PubMed: 22072503]
37. Hsieh A, Ellsworth R, Hsieh D. Hedgehog/GLI1 regulates IGF dependent malignant behaviors in glioma stem cells. J Cell Physiol. 2011; 226:1118–1127. [PubMed: 20857406]
38. Santoni M, et al. Essential role of Gli proteins in glioblastoma multiforme. Curr Protein Pept Sci. 2013; 14:133–140. [PubMed: 23544423]

39. Tremblay MR, McGovern K, Read MA, Castro AC. New developments in the discovery of small molecule Hedgehog pathway antagonists. Curr Opin Chem Biol. 2010; 14:428–435. [PubMed: 20399136]

40. NCT01576666. (on clinicaltrials.gov).

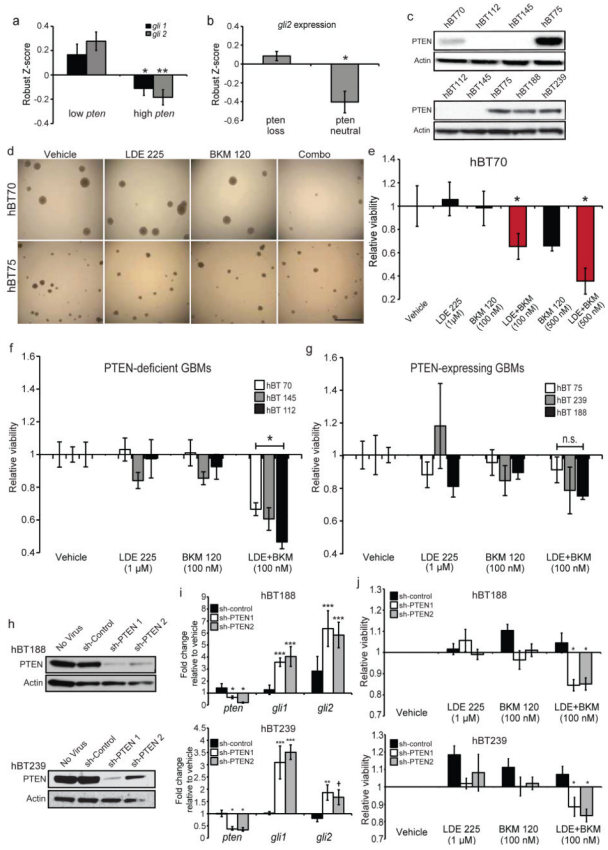

Figure 1. Coordinate activation of Shh and PI3k pathways in PTEN-deficient Glioblastoma

(**a**) *gli1*, *gli2* expression in pten-deficient and –expressing GBMs; robust z-scores for *gli1*, *gli2* (LBL database, 40% cutoff). (*) $p = 0.015$, (**) $p = 1.5 \times 10^{-6}$. (**b**) *gli2* expression and *pten* copy number (Broad database [8]). (*) $p = 0.0002$ (Supplementary Figure 1b). (**c**) PTEN Immunoblot in GBMs. Actin: loading control. (**d**) hBT70, hBT75 GBM neurospheres after treatment with Vehicle, LDE225 (1 μM), BKM120 (100 nM), or combination. Scale bar = 1 mm. (**e**) Quantification of hBT70 viability in (d). $n = 3$; two-way ANOVA factorial interaction to identify synergy in e-h, j. $F = 5.19$, $DFn = 1$, $DFd = 8$, $p = 0.0523$. (*) $F = 5.98$, $DFn = 1$, $DFd = 8$, $p = 0.0403$. (**f**) Viability of PTEN-deficient lines (hBT70, 112, 145) and therapies, $n = 3$; (*) $F = 10.27$, $DFn = 1$, $DFd = 8$, $p = 0.0125$. (**g**) Viability of PTEN-expressing lines (hBT75, 188, 239) and therapies. $n = 3$; $F = 0.09$, $DFn = 1$, $DFd = 8$, $p = 0.7749$ (n.s. = not significant). (**h**) PTEN Immunoblot in GBM cells. Actin: loading control. (**i**) *pten*, *gli1*, *gli2* mRNA normalized to *gapdh*. Results normalized to no virus, * = $p < .05$, ** = $p < .01$, *** = $p < .005$, † = 0.06. hBT188 cells ($n = 8$), For sh-control: $p = 0.36$, 0.72, 0.20 for *pten*, *gli1*, *gli2*, respectively; for sh-PTEN1 $p = 0.03$, 1.1×10^{-12}, 0.0004 for *pten*, *gli1*, *gli2*; for sh-PTEN2 $p = 0.03$, 0.0003, 9×10^{-6} for *pten*, *gli1*, *gli2*,. hBT239 cells ($n = 6$), For sh-control $p = 1.3$, 1.1, 2.72 for *pten*, *gli1*, *gli2*, respectively; sh-PTEN1 $p = 0.03$, 0.0002, 0.008 for *pten*, *gli1*, *gli2*,; for sh-PTEN2 $p = 0.03$, 4.3×10^{-14}, 0.06 for *pten*, *gli1*, *gli2*,. Z-test with Bonferroni post-test, comparison to one. (**j**) GBM response to therapies after *pten* knock-down hBT188 cells, $n = 10$, two technical replicates each in five experiments (sh-PTEN1: (*) $F = 4.69$, $DFn = 6$, $DFd = 81$, $p = 0.004$; sh-PTEN2: (*) $F = 3.10$, $DFn = 6$, $DFd = 81$, $p = 0.008$): hBT239 cells, $n = 9$, two technical replicates in three experiments (sh-PTEN1: (*) $F = 2.59$, $DFn = 6$, $DFd = 72$, $p = 0.02$; sh-PTEN2: (*) $F = 2.47$, $DFn = 6$, $DFd = 72$, $p = 0.03$). Error bars; ± S.E.M.

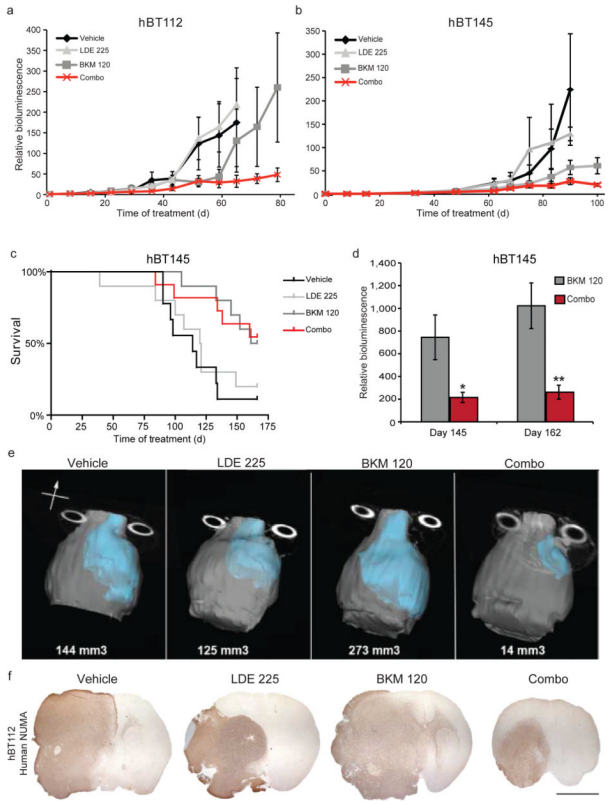

Figure 2. Combination of PI3K- and Smo-inhibition reduces tumor growth *in vivo*

(**a**) Relative bioluminescence during 80 d of treating intracranial luciferase-expressing hBT112 (n = 10 mice/group). Daily vehicle, LDE225 (60 mg kg^{-1}), BKM120 (30 mg kg^{-1}), or combination therapy. (**b**) Relative bioluminescence during 100 d of treatment in mice with luciferase-expressing hBT145 (n = 10 mice/group). Drugs above, given in cycles of 3 weeks on, 1 week off. Non-takers, non-tumor deaths censored (<1 animal per group). Treatment groups differ by two-way ANOVA ($p < 0.0001$). Combination treatment differs from BKM120 after Bonferroni post-test ($p < 0.0001$). (**c**) Kaplan-Meier analysis shows increased survival with combination therapy or BKM120, ($p < 0.0001$) by two-way ANOVA with Bonferroni post-test. (**d**) Relative bioluminescence of combination therapy and BKM120 treated mice on day 145 (BKM120, combination groups: 7 mice each), day 162 (BKM120: 4 mice; combination: 6 mice). (*) $p = 0.03$, (**) $p = 0.01$ by t-tests. (**e**) MRIs on day 65 (vehicle, LDE225), day 77 (BKM120, combination). 3-D reconstructions; tumor tissue (blue), arrowhead: anterior, tumor volumes indicated. (**f**) Immunostaining for human NuMA shows tumor cells within mouse brain (day 65 for vehicle, LDE225, day 80 for BKM120, combination). Scale bar = 5mm.

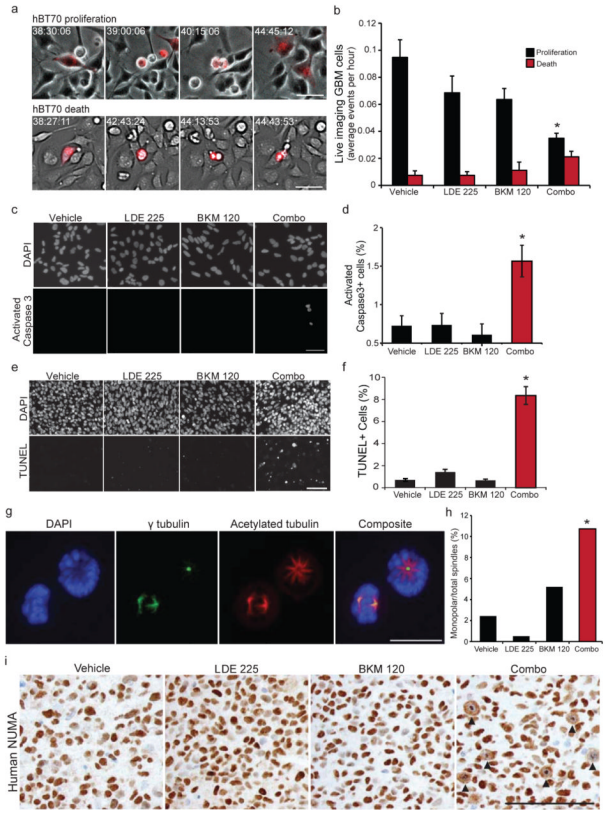

Figure 3. Cellular basis for efficacy of combination treatment

(**a**) Time-lapse imaging (120 h) of hBT70 cells. Time after drug application in hh:mm:ss, Scale bar = 25μm. (**b**) Data from 60 cells per condition, three technical replicates, $p = 0.0045$ by one-way ANOVA. (*) $p < 0.05$ with Bonferroni post-test. (**c**) Immunostaining for activated caspase-3 in hBT70, DAPI nuclear staining, Scale bar = 50μm. (**d**) Apoptotic index increased in combination therapy, $n = 3$; $p < 0.0001$ by one-way ANOVA, (*) $p < 0.05$ with Bonferroni post-test. (**e**) TUNEL staining in hBT112 xenografts, DAPI nuclear staining, Scale bar = 50μM. (**f**) Apoptotic index *in vivo* increased in combination therapy, N ≥ 2000 cells per condition, $p < 0.0001$ by one-way ANOVA, (*) $p < 0.05$ after Bonferroni post-test. (**g**) hBT70 treated, stained for DAPI (blue), γ tubulin (centrosomes; green), acetylated tubulin (spindles; red). Monopolar spindle (right) and normal, bipolar spindle (left). Scale bar = 10μm. (**h**) Monopolar spindles increased with combination therapy. ≥ 261 cells per treatment, in two independent experiments, (*) $p < 0.001$ by chi-square. (**i**) Immunostaining for human NuMA in hBT112 xenografts. Arrowheads indicate abnormal mitoses, Scale bar = 50μM. Error bars; ± S.E.M.

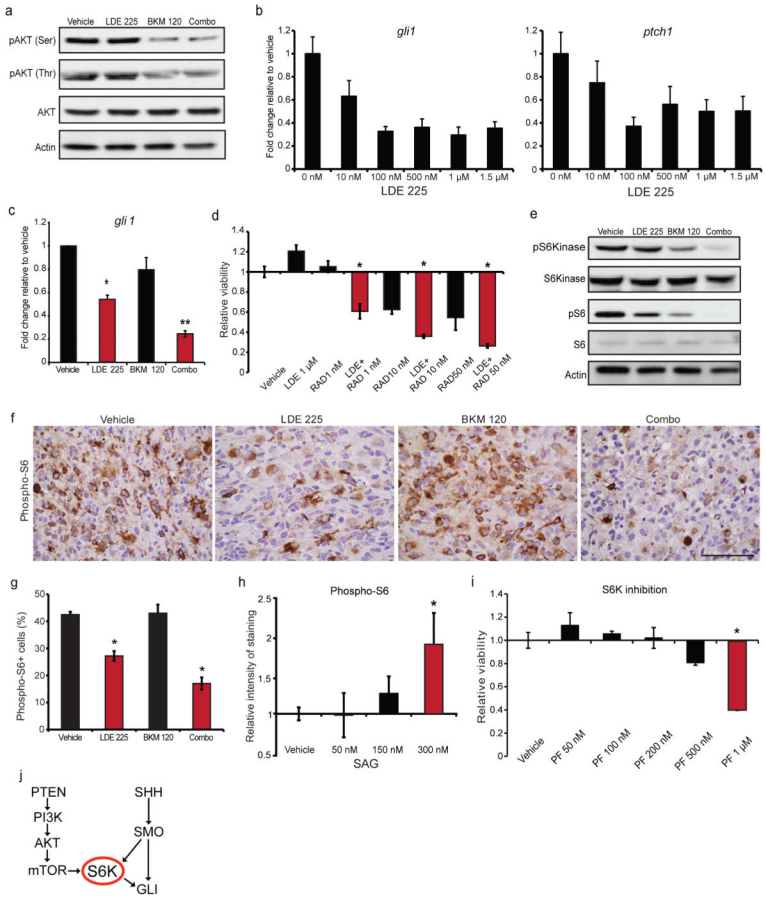

Figure 4. Combination therapy targets PI3k, Shh and S6k pathways

(**a**) Immunoblots of phosphorylated and total AKT in hBT112 treated with LDE225 (1 μM), BKM120 (500 nM), combination therapy, Actin: loading control. (**b**) *gli1*, *ptch1* mRNA levels normalized to *gapdh* ($n = 3$): Error bars; +/− SEM, $p < 0.05$ by one-way ANOVA, Tukey post-test. (**c**) *gli1* mRNA levels normalized to *gapdh* ($n = 3$): Error bars; +/− SEM, (*) $p \leq 0.005$ by z-test compared to one: (**) $p < 0.05$ by one-way ANOVA, Tukey post-test. (**d**) Combination treatment with RAD001 (1 nM, 10 nM, 50 nM), and LDE225 (1 μM) synergistically reduces viability of hBT70 ($n = 3$), two-way ANOVA factorial interaction (*) $F = 10.45$, $DFn = 3$, $DFd = 16$, $p = 0.0005$. (**e**) Immunoblots of phosphorylated and total S6K, S6 from hBT112, Actin: loading control. (**f**) Immunostaining of phosphorylated S6 (pS6) in hBT112 xenografts after 65 d (vehicle, LDE225), 77 days treatment (BKM120, combination). Scale bar = 50μm. (**g**) pS6-positive cells decreases with LDE225, combination therapy *in vivo*. Data represent ≥ 900 cells per condition, (*) $p = 0.0003$ by chi-square, Bonferroni post-test. (**h**) SAG increases pS6 intensity per cell increases in hBT112. Means of ≥ 1944 cells from three independent experiments. (*) $p = 0.01$ by one-way ANOVA with Tukey post-test. (**i**) hBT112 shows decreased viability ($n = 3$): (*) $p < 0.05$ by one-way ANOVA with Bonferroni post-test. (**j**) Model of interaction between PI3K, Shh pathways in PTEN-deficient GBMs. Error bars; ± S.E.M.